NANO LETTERS

Letter

Determination of the Young's Modulus of Structurally Defined Carbon Nanotubes

Yang Wu, Mingyuan Huang, Feng Wang, X. M. Henry Huang, Sami Rosenblatt, Limin Huang, Hugen Yan, Stephen P. O'Brien, James Hone, and Tony F. Heinz

Nano Lett., **2008**, 8 (12), 4158-4161 • Publication Date (Web): 30 October 2008

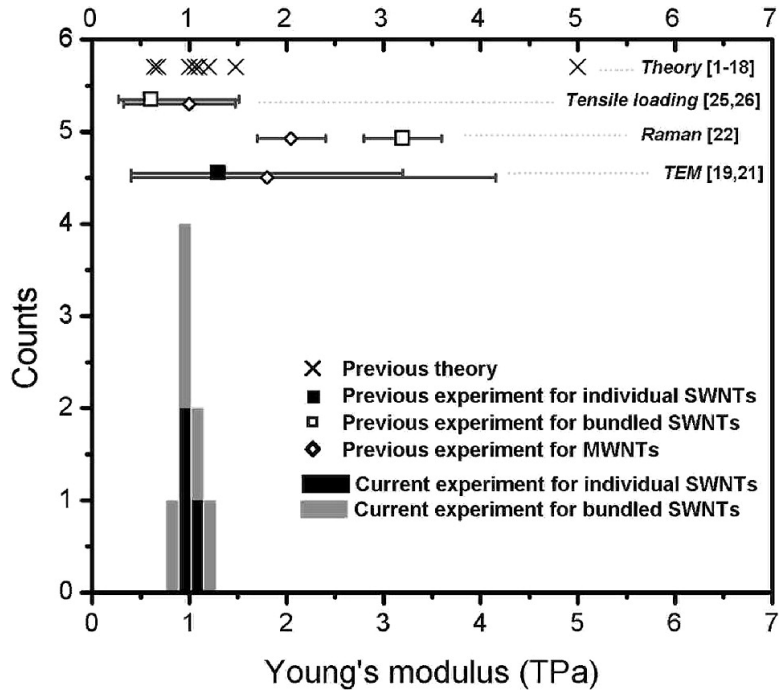

More About This Article

Additional resources and features associated with this article are available within the HTML version:

- Supporting Information
- Access to high resolution figures
- Links to articles and content related to this article
- Copyright permission to reproduce figures and/or text from this article

NANO LETTERS

2008
Vol. 8, No. 12
4158-4161

Determination of the Young's Modulus of Structurally Defined Carbon Nanotubes

Yang Wu,[†] Mingyuan Huang,[‡] Feng Wang,[†,§] X. M. Henry Huang,[‡] Sami Rosenblatt,[†] Limin Huang,[||] Hugen Yan,[†] Stephen P. O'Brien,[||] James Hone,[‡] and Tony F. Heinz[†,*]

Departments of Physics, Electrical Engineering, Mechanical Engineering, and Applied Physics and Applied Mathematics, Columbia University, New York, New York 10027

Received June 1, 2008; Revised Manuscript Received September 20, 2008

ABSTRACT

We have combined optical characterization with a magnetic actuation technique to measure the stiffness of single-walled carbon nanotubes of defined crystal structure. The measured stiffnesses correspond to an average Young's modulus of $E = 0.97 \pm 0.16$ TPa. For the structures investigated, no dependence on the nanotube chiral index was observed within the indicated experimental accuracy.

The attractive mechanical properties of carbon nanotubes have stimulated active theoretical[1−18] and experimental[19−28] research and have also permitted the demonstration of distinctive nanomechanical devices.[29−34] In particular, the stiffness of single-walled nanotubes (SWNTs) under tensile strain is known to be unusually high. Experimental measurements of the Young's modulus E indicate a value on the order of 1 TPa. Reported values of this fundamental material property have, however, shown variations up to an order of magnitude, in large part because of the difficulty in determining the precise structure of the nanotube or nanotubes under study. It has therefore been difficult to ascertain experimentally whether there exists a significant intrinsic dependence of mechanical properties on the nanotube crystallographic structure. Here we combine optical characterization of individual single-walled nanotubes with a magnetic actuation technique to measure the Young's modulus of nanotubes of known chiral index. We obtain an average value for the different single-walled carbon nanotubes of $E = 0.97 \pm 0.16$ TPa, a result close to the in-plane Young's modulus of graphite. Within the indicated experimental accuracy, we do not observe variation in the Young's modulus for the individual nanotubes characterized in this investigation. Measurements of the average Young's modulus of nanotubes forming small bundles of two or three nanotubes are also consistent with this value.

The arrangement of the nanotube samples for our combined structural characterization by optical spectroscopy and mechanical characterization by magnetic actuation is depicted in Figure 1. Both the optical and mechanical properties of the individual nanotubes were investigated using isolated SWNTs suspended over an open slit. The substrate for these studies was a silicon wafer with Si_3N_4 epilayers on both sides. A large slit (100 μm wide and 1.2 mm long) through this substrate was produced by photolithography and wet etching. The SWNTs for this study were prepared by chemical vapor deposition (CVD) using ethanol as a feedstock[35] and an ultrathin film ($\sim$0.5 nm) of Co, evaporated on the substrate, as the catalyst. The process produced a low density of long SWNTs, aligned by the flow of the reactor gas, that spanned the slit [Figure 1a]. An array of gold pads (100 μm wide) was deposited on opposite sides of the slit by thermal evaporation through a shadow mask [Figure 1b]. The pads affixed the nanotubes securely to the substrate and also served as electrodes to allow us to pass current through individual nanotubes. The shadow mask used to prepare these features was affixed to the chip under an optical microscope and provided alignment of the pads to the slit edge to within $\sim$2 μm.

Rayleigh (elastic) scattering spectroscopy was applied for optical characterization of the individual nanotubes suspended over the slit[36] [Figure 1c]. The Rayleigh spectra revealed the energies of the electronic transitions of the SWNTs, from which reliable assignments of the nanotube chiral indices could be made.[37] The spectra also permitted us to discriminate between individual nanotubes and small bundles of a few nanotubes.

* Corresponding author. E-mail: tony.heinz@columbia.edu.
[†] Departments of Physics and Electrical Engineering.
[‡] Department of Mechanical Engineering.
[§] Current Address: Dept. of Physics, University of California, Berkeley, CA 94720.
[||] Department of Applied Physics and Applied Mathematics.

10.1021/nl801563q CCC: $40.75
Published on Web 10/30/2008

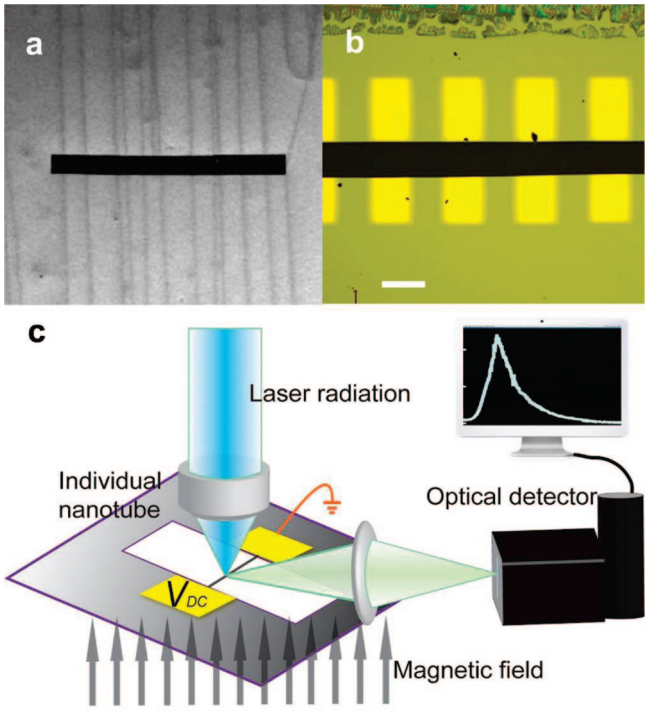

Figure 1. Experimental samples and arrangement: (a) scanning electron microscope image of the sample, showing the Si substrate with several SWNTs traversing the open slit; (b) optical image of the sample after the deposition of gold electrodes on each side of the slit; the scale bar indicates a length of 100 μm; (c) schematic representation of the overall experimental arrangement for the determination of the Young's modulus of nanotubes of known chiral index. The schematic diagram shows the arrangement for magnetic actuation of the nanotube by a Lorentz force, for the measurement of the nanotube spectrum by Rayleigh scattering spectroscopy with a continuum laser source, and for the determination of the nanotube spatial position by light scattering of a monochromatic laser with its tight focus slightly displaced from the position of the nanotube.

Once the chiral indices of an individual SWNT had been determined, we examined mechanical properties of the nanotube by subjecting it to a calibrated transverse force and measuring the resulting transverse displacement. The force on a suspended nanotube was produced by passing a current through it in the presence of a perpendicular magnetic field. The resulting Lorentz force per unit length was then given simply by the product of the current and the magnetic field strength. The magnetic field was produced by a permanent magnet and had a strength of $B = 0.31$ T at the slit, as measured by a Hall sensor (SMS 102, TEL-Atomic Inc.). The strain of the nanotube resulting from the applied force was determined by measuring its lateral displacement. This was achieved by monitoring the intensity of light scattered from the nanotube in the presence of the spatially varying field of a continuous-wave 532 nm laser. The laser beam was focused ($\sim$2 μm diameter) slightly to the side of the nanotube to give maximum sensitivity to small displacements. We directly calibrated the relationship between the displacement of the nanotube and the intensity of the scattered light by scanning the sample laterally in 100-nm steps with a precision translation stage. To increase the scattering intensity and thus the signal-to-noise ratio of the measurement, a thin gold layer of 1 μm length was evaporated onto a segment of each nanotube at the center of the slit. Because of the resulting enhanced scattering, a laser intensity of only 5 μW was sufficient for accurate measurement of the nanotube position.

Figure 2 shows the measured lateral displacement as a function of the applied transverse force for three different individual SWNTs and one bundle of two semiconducting SWNTs. The insets display the corresponding Rayleigh scattering spectra, from which the indicated nanotube chiral indices were deduced. Determination of the chiral indices yields a precise value for the nanotube diameter for our analysis of the Young's modulus. In the case of bundles, which constitute the majority of samples characterized by Rayleigh spectroscopy, we were not able to assign the chiral indices unambiguously. In bundles of two semiconducting nanotubes, as shown in Figure 2d, we observe four peaks (two per nanotube), which can be assigned to the two constituent nanotubes in three possible combinations. However, because the diameter of each semiconducting nanotube is a function of the average position of the two peaks, the average nanotube diameter in the bundle is nearly the same for each combination. For example, for the bundle shown in the figure, the three possible assignments give average diameters of 1.90, 1.90, and 1.95 nm. The spread in these values ($\sim$2.5%) is significantly smaller than the uncertainty in our experimental determination of the Young's modulus.

As illustrated in Figure 2, two characteristic forms of response of an isolated nanotube to an applied force are observed. In the first type of behavior [Figure 2a], an abrupt displacement as large as 200 nm occurs upon the application of a small force. In the second type [Figure 2b,c], we see a gradually varying displacement under the applied force. In both cases, away from the point of zero force, the displacement rises steadily with force, displaying a weak saturation for large applied forces. All observed forms of the nanotube mechanical response can be described within the model of a classical string, if we include a suitable amount of initial slack or tension. The string model is appropriate for a material with a finite Young's modulus for stretching but negligible flexure stiffness. This condition is satisfied for the long ($\sim$100 μm) and narrow ($\sim$2 nm) nanotubes under study here.

Within this picture, the relation between the (homogeneously) applied lateral force F and the displacement y at the center of a suspended nanotube is given in terms of its Young's modulus E by[38]

$$F = 8\frac{AE}{L}y \max\left[0, \frac{8}{3}\left(\frac{y}{L}\right)^2 + \varepsilon_0\right] \quad (1)$$

Here L and A represent the nanotube's length and effective area, respectively, and ε_0 denotes its strain in the absence of an applied force. For a nanotube with initial slack ($\varepsilon_0 < 0$), a small lateral force will immediately drive it to a taut state. This produces an abrupt displacement when a slight force is applied, corresponding to the first type of behavior described above [Figure 2a]. For nanotubes initially under tensile strain ($\varepsilon_0 > 0$), the lateral displacement varies smoothly with

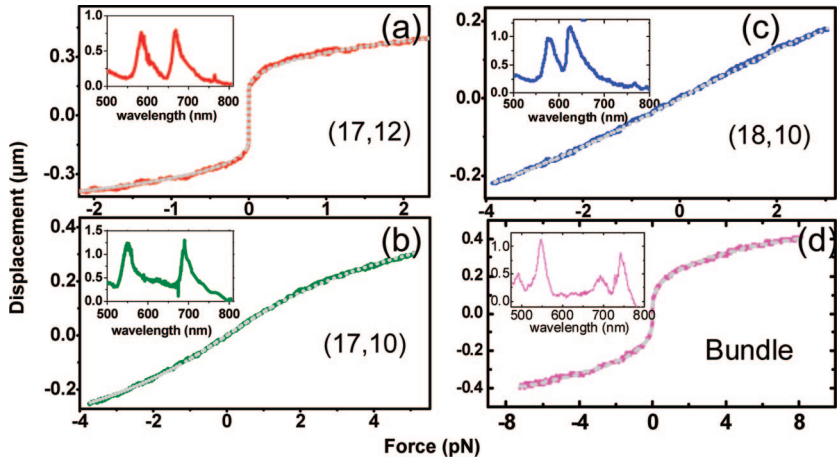

Figure 2. Experimental results (solid lines) for the lateral displacement versus the applied lateral force for three different individual SWNTs and one bundle consisting of two nanotubes. The predicted displacements from the model presented in the text are shown as dotted lines. The different types of behavior seen in the top panel and in the lower two panels result, respectively, from initial slack or tension in the SWNTs. The insets are the measured Rayleigh scattering spectra for each nanotube, from which the indicated index assignments are obtained.

Table 1. Summary of Results for the Individual Nanotubes in Figure 2[a]

nanotube	E_{33} (eV)	E_{44} (eV)	chiral indices (n, m)	diameter (nm)	chiral angle (deg)	initial strain ε_0	tube length L (μm)	E (TPa)
1	1.86	2.12	(17,12)	2.00	24.3	-2.2×10^{-5}	92	0.93 ± 0.16
2	1.80	2.30	(17,10)	1.88	21.5	5.7×10^{-5}	91	1.03 ± 0.16
3	1.96	2.17	(18,10)	1.95	20.6	8.9×10^{-5}	94	0.94 ± 0.16

[a] The chiral index assignments are based on the indicated energies of the third and fourth sub-band transitions, as obtained from the Rayleigh scattering spectra. These (n, m) indices yield the nanotube diameter and chiral angle, as shown. The initial strain ε_0 and the Young's modulus E are determined by fitting the experimental force−displacement data using the model described in the text. The estimated uncertainty for the Young's modulus includes systematic error from uncertainty of the strength of magnetic field, misalignment of the contact pads with the slit, and the possible influence of Joule heating.

applied force, corresponding to the second type of behavior [Figure 2b,c].

Excellent agreement is obtained between all experimental force-displacement relations and the predictions of the string model (dotted curves in Figure 2). The theoretical predictions for displacement were broadened by 80 nm to account for the jitter in the experimental determination of measurement of the nanotube position. The fits of the experimental force−displacement relations to the model involve only two unknown parameters, the Young's modulus E and initial strain ε_0 of the nanotube under study. All of the other parameters in eq 1 are determined by the experiment. In particular, the length of the nanotube is fixed by the experimental geometry; the effective nanotube area is obtained from the experimentally deduced nanotube chiral indices and an assumed nanotube wall thickness of 0.34 nm corresponding to the interlayer spacing in graphite.

For the single nanotubes of Figures 2a−c, we obtain, respectively, Young's moduli of 0.93, 1.03, and 0.94 TPa. For the five small bundles of nanotubes that were studied, we deduced average Young's moduli of 0.80, 1.05, 1.00, 0.96, and 1.25 TPa. The measurements of the individual nanotubes thus yielded a mean value for the Young's modulus of $E = 0.97$ TPa, with a standard deviation of 0.05 TPa. Including the five bundles (weighted equally) in the average, we obtain a mean value of $E = 0.99$ TPa, with a standard deviation of 0.13 TPa. The fits also provide information about the initial extension of each nanotube, as indicated in Table 1. The corresponding values of the initial strain ε_0 are less than 10^{-4} and reflect experimental variation in the growth and sample fabrication process.

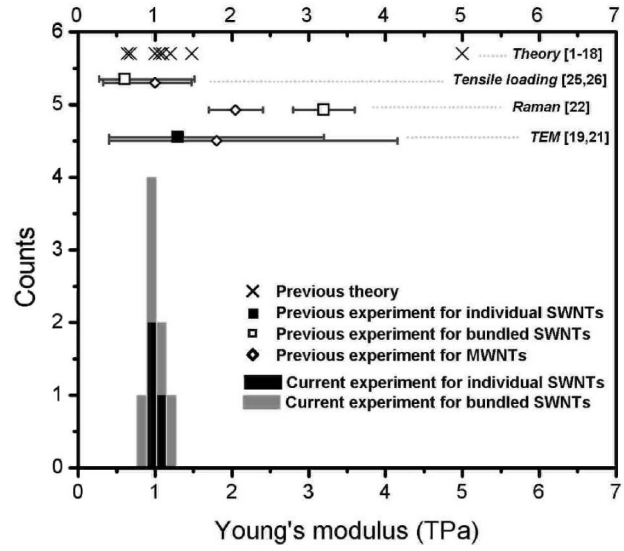

Figure 3. Values of the Young's modulus for carbon nanotubes from this study and previous experimental and theoretical investigations. The results of the current experiment for both individual (black bars) SWNTs and bundles of just two SWNTs (gray bars) are plotted as a histogram. The other symbols in the figure summarize literature values and illustrate the wide dispersion of experimental and theoretical results for single-walled and multi-walled carbon nanotubes (MWNTs). The values of Young's modulus from the literature are consistently presented using an effective nanotube area based on a wall thickness of 0.34 nm.

We now consider the accuracy of our measurements of the Young's modulus. There are three principal sources of experimental uncertainty. The first arises from the inaccuracy in determining the magnetic field strength at the location of the nanotube. Possible spatial variation in the field strength leads to an uncertainty of 10%. The second source of uncertainty arises from modest heating of the nanotube by the electrical current used for magnetic actuation. From the electrical power dissipation and the nanotube thermal expansion coefficient,[39] we estimate this error does not exceed 10%. The third source is an estimated 2% uncertainty in the effective length of the nanotube from potential misalignment of the gold electrodes to the slit edge. This contributes a 6% uncertainty to the determination of E, which (for large applied force) is cubic in the nanotube length. Combining these independent uncertainties in quadrature, we obtain an estimated accuracy for measurements of individual nanotubes of 16%.

Figure 3 summarizes the results of the measurements of the three individual nanotubes and of the five bundles. As indicated above, the average Young's modulus of the entire data set was 0.99 TPa, with a standard deviation of 0.13 TPa, while the results for the subset of individual nanotubes yields a mean Young's modulus of 0.97 TPa with a standard deviation of 0.05 TPa. Both of these mean values are very close to the measured value of 1.02 TPa for the in-plane Young's modulus of graphite.[40] As the figure shows, our value for the Young's modulus falls in the same range as previous experimental studies but with significantly smaller uncertainty. For this subset of nanotubes, all with diameters near 2 nm, the dependence of the Young's modulus on the chiral index is clearly smaller than the measurement uncertainty of 16%. This result is consistent with theoretical predictions, which generally predict a variation of Young's modulus with chiral indices of less than 10%.[1−18] Further improvements to the experimental measurement technique, such as the use of a magnet with a larger and more homogeneous field, should permit a more stringent test of predicted dependence of the Young's modulus on the nanotube crystallographic structure.

Acknowledgment. We acknowledge support from the Nanoscale Science and Engineering Initiative of the NSF (NIRT Grant ECS-05-07111), the DARPA Center on Nanoscale Science and Technology for Integrated Micro/Nano-Electromechanical Transducers (iMINT Grant HR0011-06-1-0048), and the Office of Basic Energy Sciences, U.S. DOE (Grant DE-FG02-03ER15463).

References

(1) Robertson, D. H.; Brenner, D. W.; Mintmire, J. W. *Phys. Rev. B* **1992**, *45*, 12592–12595.
(2) Overney, G.; Zhong, W.; Tomanek, D. *Z. Phys. D* **1993**, *27*, 93.
(3) Gao, G. H.; Cagin, T.; Goddard, W. A. *Nanotechnology* **1998**, *9*, 184–191.
(4) Yao, N.; Lordi, V. *J. Appl. Phys.* **1998**, *84*, 1939–1943.
(5) Salvetat, J. P.; Bonard, J. M.; Thomson, N. H.; Kulik, A. J.; Forro, L.; Benoit, W.; Zuppiroli, L. *Appl. Phys. A: Mater. Sci. Process.* **1999**, *69*, 255–260.
(6) Popov, V. N.; Van Doren, V. E.; Balkanski, M. *Phys. Rev. B* **2000**, *61*, 3078–3084.
(7) Van Lier, G.; Van Alsenoy, C.; Van Doren, V.; Geerlings, P. *Chem. Phys. Lett.* **2000**, *326*, 181–185.
(8) Zhou, X.; Zhou, J. J.; Ou-Yang, Z. C. *Phys. Rev. B* **2000**, *62*, 13692–13696.
(9) Tu, Z. C.; Ou-Yang, Z. *Phys. Rev. B* **2002**, *65*, 233407.
(10) Wang, J. B.; Guo, X.; Zhang, H. W.; Wang, L.; Liao, J. B. *Phys. Rev. B* **2006**, *73,* 119901.
(11) Sun, C. H.; Li, F.; Cheng, H. M.; Lu, G. Q. *Appl. Phys. Lett.* **2005**, *87,* 193101.
(12) Sawaya, S.; Akita, S.; Nakayama, Y. *Nanotechnology* **2007**, *18*, 035702.
(13) Pullen, A.; Zhao, G. L.; Bagayoko, B.; Yang, L. *Phys. Rev. B* **2005**, *71*, 205410.
(14) Mylvaganam, K.; Zhang, L. C. *Carbon* **2004**, *42*, 2025–2032.
(15) Hernandez, E.; Goze, C.; Bernier, P.; Rubio, A. *Appl. Phys. A: Mater. Sci. Process.* **1999**, *68*, 287–292.
(16) Gupta, S.; Dharamvir, K.; Jindal, V. K. *Phys. Rev. B* **2005**, *72*, 165428.
(17) Cai, J.; Bie, R. F.; Tan, X. M.; Lu, C. *Physica B* **2004**, *344*, 99–102.
(18) Bao, W. X.; Zhu, C. C.; Cui, W. Z. *Physica B* **2004**, *352*, 156–163.
(19) Treacy, M. M. J.; Ebbesen, T. W.; Gibson, J. M. *Nature* **1996**, *381*, 678–680.
(20) Wong, E. W.; Sheehan, P. E.; Lieber, C. M. *Science* **1997**, *277*, 1971–1975.
(21) Krishnan, A.; Dujardin, E.; Ebbesen, T. W.; Yianilos, P. N.; Treacy, M. M. J. *Phys. Rev. B* **1998**, *58*, 14013–14019.
(22) Lourie, O.; Wagner, H. D. *J. Mater. Res.* **1998**, *13*, 2418–2422.
(23) Salvetat, J. P.; Briggs, G. A. D.; Bonard, J. M.; Bacsa, R. R.; Kulik, A. J.; Stockli, T.; Burnham, N. A.; Forro, L. *Phys. Rev. Lett.* **1999**, *82*, 944–947.
(24) Poncharal, P.; Wang, Z. L.; Ugarte, D.; de Heer, W. A. *Science* **1999**, *283*, 1513–1516.
(25) Yu, M. F.; Lourie, O.; Dyer, M. J.; Moloni, K.; Kelly, T. F.; Ruoff, R. S. *Science* **2000**, *287*, 637–640.
(26) Yu, M. F.; Files, B. S.; Arepalli, S.; Ruoff, R. S. *Phys. Rev. Lett.* **2000**, *84*, 5552–5555.
(27) Ruoff, R. S.; Qian, D.; Liu, W. K. *C. R. Phys.* **2003**, *4*, 993–1008.
(28) Cuenot, S.; Fretigny, C.; Demoustier-Champagne, S.; Nysten, B. *J. Appl. Phys.* **2003**, *93*, 5650–5655.
(29) Fennimore, A. M.; Yuzvinsky, T. D.; Han, W. Q.; Fuhrer, M. S.; Cumings, J.; Zettl, A. *Nature* **2003**, *424*, 408–410.
(30) Sazonova, V.; Yaish, Y.; Ustunel, H.; Roundy, D.; Arias, T. A.; McEuen, P. L. *Nature* **2004**, *431*, 284–287.
(31) Papadakis, S. J.; Hall, A. R.; Williams, P. A.; Vicci, L.; Falvo, M. R.; Superfine, R.; Washburn, S. *Phys. Rev. Lett.* **2004**, *93*, 146101.
(32) Nishio, M.; Sawaya, S.; Akita, S.; Nakayama, Y. *Appl. Phys. Lett.* **2005**, *86*, 133111.
(33) Lu, D. Y.; Li, Y.; Ravaioli, U.; Schulten, K. *Phys. Rev. Lett.* **2005**, *95*, 246801.
(34) Jensen, K.; Girit, C.; Mickelson, W.; Zettl, A. *Phys. Rev. Lett.* **2006**, *96*, 215503.
(35) Huang, L. M.; Cui, X. D.; White, B.; O'Brien, S. P. *J. Phys. Chem. B* **2004**, *108*, 16451–16456.
(36) Sfeir, M. Y.; Wang, F.; Huang, L. M.; Chuang, C. C.; Hone, J.; O'Brien, S. P.; Heinz, T. F.; Brus, L. E. *Science* **2004**, *306*, 1540–1543.
(37) Sfeir, M. Y.; Beetz, T.; Wang, F.; Huang, L. M.; Huang, X. M. H.; Huang, M. Y.; Hone, J.; O'Brien, S.; Misewich, J. A.; Heinz, T. F.; Wu, L. J.; Zhu, Y. M.; Brus, L. E. *Science* **2006**, *312*, 554–556.
(38) Dickey, R. W. *SIAM J. Appl. Math.* **1969**, *17*, 172.
(39) Kwon, Y. K.; Berber, S.; Tomanek, D. *Phys. Rev. Lett.* **2004**, *92*, 015901.
(40) Blakslee, O. L.; Proctor, D. G.; Sheldin, E. J.; Spence, G. B.; Weng, T. *J. Appl. Phys.* **1970**, *41*, 3373.

NL801563Q